Headline Articles

Magnetic Studies on Quaternary Iron Sulfides BaLn$_2$FeS$_5$ (Ln = Ce, Pr, Nd, Sm) by Magnetic Susceptibility, Specific Heat, ^{57}Fe Mössbauer Spectrum, and Neutron Diffraction Measurements

Makoto Wakeshima,* **Kentaro Ino, Yukio Hinatsu, and Yoshinobu Ishii**[†]

Division of Chemistry, Graduate School of Science, Hokkaido University, Sapporo 060-0810

†Japan Atomic Energy Research Institute, Tokai-mura, Ibaraki 319-1195

Magnetic properties of quaternary iron sulfides, BaLn$_2$FeS$_5$ (Ln = Ce, Pr, Nd, Sm), have been investigated through magnetic susceptibility, electrical resistivity, specific heat, ^{57}Fe Mössbauer spectrum, and powder neutron diffraction measurements. In these compounds, the Fe^{2+} ion exhibits an antiferromagnetic ordering at around 40 K. In the Nd and Sm compounds, these lanthanide ions show an antiferromagnetic ordering at 6.5 K for Ln = Nd and at 28 K for Ln = Sm. The reduction of the Fe^{2+} magnetic moment is observed below 120–170 K for all the compounds. Their electrical conductivities show an Arrhenius temperature-dependence, and the activation energies change at around the moment-reduction temperatures. The ^{57}Fe Mössbauer spectra for BaPr$_2$FeS$_5$ indicate that the FeS$_4$ tetrahedron is distorted prominently below the temperature at which both the magnetic susceptibility and the electrical resistivity show an anomaly in their temperature dependence. The neutron diffraction data collected for BaPr$_2$FeS$_5$ at 10 K show that it has a collinear antiferromagnetic structure and that the magnetic moments of the Fe^{2+} ions are parallel to the *c*-axis.

Many binary and ternary chalcogenides containing rare earths have been synthesized.[1] These compounds adopt a wide range of structure types and show a variety of interesting physical properties.[2] However, studies on quaternary rare-earth chalcogenides are still scarce compared with the case for binary and ternary chalcogenides.[3–8]

A quaternary manganese sulfide, BaLa$_2$MnS$_5$, was first synthesized by Masuda et al.[9] Recently, our research group has reported the synthesis, crystal structures and magnetic properties of a new series of quaternary sulfides BaLn$_2$TS$_5$ (Ln = La, Ce, Pr, Nd; T = Mn, Co, Zn).[10–12] These sulfides crystallize in a tetragonal structure (space group *I*4/*mcm*) based on the stacking of BaTS$_4$ and Ln$_2$S layers. Figure 1 shows the schematic crystal structure of BaLn$_2$TS$_5$. In the BaTS$_4$ layer, the T ion is bonded to four sulfur ions in a tetrahedral coordination and these TS$_4$ tetrahedra link via the Ba ions. The electrical conductivity of BaLa$_2$MnS$_5$ was reported to be semiconductive.[9] The magnetic properties of BaLn$_2$TS$_5$ (T = Mn, Co) indicated an antiferromagnetic ordering of the Mn^{2+} and Co^{2+} ions below ca. 60 K.[10–12] Furthermore, the Nd compounds, BaNd$_2$TS$_5$ (T = Mn, Co, Zn), also showed the antiferromagnetic transition of the Nd^{3+} ions below ca. 5 K.[12]

In our previous work, several new quaternary iron sulfides BaLn$_2$FeS$_5$ (Ln = La, Ce, Pr, Nd, Sm) were synthesized, and their crystal structures were determined to be isostructural
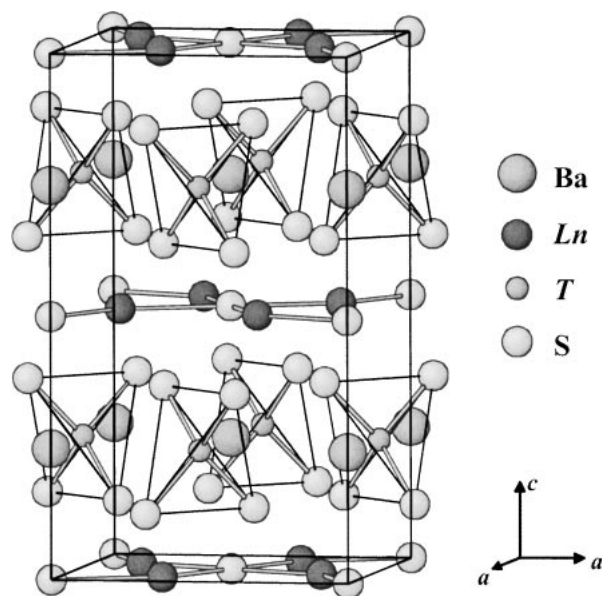
Fig. 1. Schematic crystal structure of BaLn$_2$TS$_5$.

with the BaLn$_2$TS$_5$ (T = Mn, Co, Zn).[13] Among them, BaLa$_2$FeS$_5$ exhibited a spin-glass like behavior below 22 K. The results of the magnetic susceptibility measurements show that the divalent Fe ions are in a high-spin state.[14] In this

study, we focus our attention on the BaLn$_2$FeS$_5$ family (Ln = Ce, Pr, Nd, Sm) in which both the Ln^{3+} and Fe^{2+} ions are magnetic. Their physical properties has been investigated through their magnetic susceptibility, specific heat, electrical resistivity, ^{57}Fe Mössbauer spectrum, and powder neutron diffraction measurements.

Experimental

Four quaternary iron sulfides, BaLn$_2$FeS$_5$ (Ln = Ce, Pr, Nd, Sm), were synthesized by a solid-state reaction. Barium sulfide (BaS), iron monosulfide (FeS), and lanthanide sulfides (Ln$_2$S$_3$ (Ln = Ce, Pr, Nd, Sm)) were used as starting materials. In order to obtain lanthanide sulfides and barium sulfide, lanthanide oxides and barium carbonate were heated in a graphite boat at 1000 °C in a flow of the mixed gas of CS$_2$ and N$_2$ which was obtained by bubbling the N$_2$ gas through liquid CS$_2$ at room temperature. The starting materials were stoichiometrically mixed together in a globe box and then sealed in an evacuated silica tube. The tube was heated at 900 °C (BaCe$_2$FeS$_5$), or 950 °C (BaPr$_2$FeS$_5$, BaNd$_2$FeS$_5$, BaSm$_2$FeS$_5$) for 3 days, with regrinding at intervals.

The magnetic susceptibilities were measured under an applied field of 0.1 T in the temperature range between 2 and 300 K by using a SQUID magnetometer (Quantum Design, MPMS-5S).

The temperature dependence of the electrical resistivity was measured by four-probe dc techniques in the temperature range between 70 and 300 K.

Specific heat measurements were carried out using a relaxation technique supplied by the commercial specific heat measurement system (Quantum Design, PPMS) in the temperature range from 1.8 to 300 K. The sample in the form of a pellet (∼7 mg) was mounted on an alumina plate with apiezon for better thermal contact.

The ^{57}Fe Mössbauer spectrum was measured in the temperature range from 50 to 300 K with a Mössbauer spectrometer VT-6000 (Laboratory Equipment Co.) using a radiation source ^{57}Co(Rh). The sample lapped in an aluminum foil was cooled down to each temperature by using the variable temperature cryostat system CryoMini (Iwatani Industrial Gases Co.). The spectrometer was calibrated using α-Fe at room temperature and the isomer shift was determined relative to the shift of α-Fe.

The powder neutron diffraction profiles were measured at 10, 100 and 200 K using a high-resolution powder diffractometer (HRPD) at JRR-3M reactor (Japan Atomic Energy Research Institute)[15] with a Ge (331) monochromator (λ = 1.8230 Å) in the 2θ range from 0.05 to 165° using a 2θ step size of 0.05°. The collimators used were 6'-20'-6', these were placed before and after the monochromator, and between the sample and each detector. The set of 64 detectors and collimators were placed at every 2.5° of diffraction angle, and the set rotates around the sample. The sample was contained in a vanadium can with 10 mm diameter and 45 mm height, and was measured at 10, 100 and 200 K. The Rietveld method was applied to the intensity data from 2θ = 5 to 150° for the crystal and magnetic structure refinements, using the program RIETAN-2000.[16]

Results and Discussion

Magnetic Susceptibilities. Figure 2(a) shows the magnetic susceptibilities as a function of temperature for BaLn$_2$FeS$_5$ (Ln = Ce, Pr, Nd, Sm) below 60 K. For all the compounds, their susceptibilities indicate that an antiferromagnetic transition occurs at around 40 K. These transitions are attributable
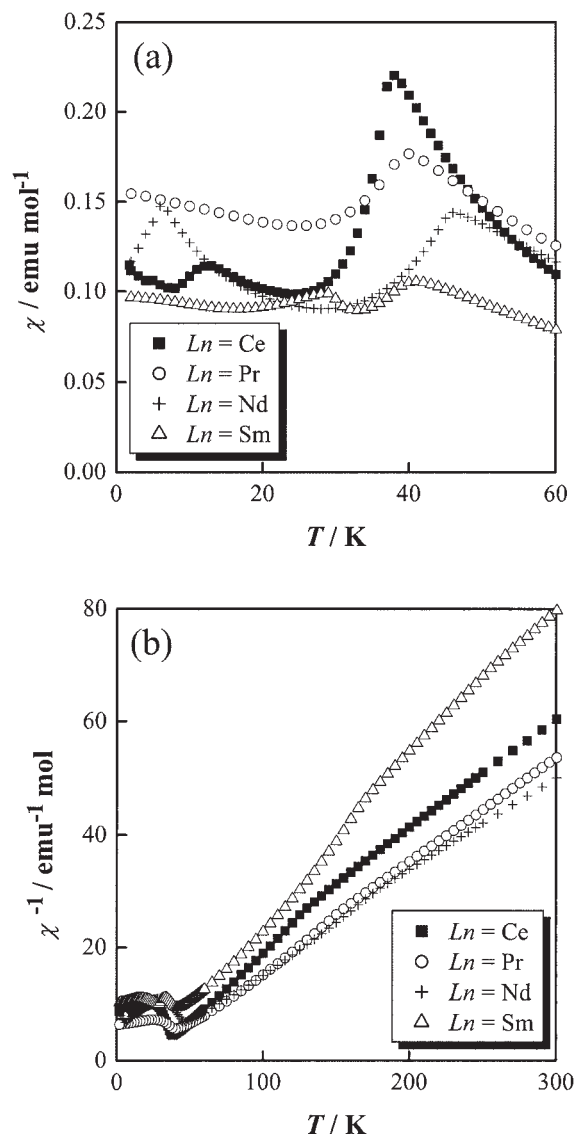

Fig. 2. (a) Temperature dependence of magnetic susceptibilities for BaLn$_2$FeS$_5$ (Ln = Ce, Pr, Nd, Sm) below 60 K: (b) Temperature dependence of reciprocal magnetic susceptibilities for BaLn$_2$FeS$_5$ (Ln = Ce, Pr, Nd, Sm) below 300 K.

to the antiferromagnetic orderings of the Fe^{2+} moments, because the transition temperatures are independent of the kinds of Ln ions. Such magnetic behavior of the Fe ions is analogous with those of the Mn and Co ions for BaLn$_2$TS$_5$ (T = Mn, Co), which are antiferromagnetic below ca. 60 K.[11,13] It was found that the Nd and Sm compounds show another antiferromagnetic transition at 6.5 and 28 K, respectively. For other isostructural Nd compounds, BaNd$_2$TS$_5$ (T = Mn, Co, Zn), the antiferromagnetic orderings of the Nd^{3+} moments have been observed below ca. 5 K.[13] Therefore, the antiferromagnetic transition at 6.5 K found for BaNd$_2$FeS$_5$ should similarly be due to the antiferromagnetic coupling of the Nd ions.

Figure 2(b) shows the temperature dependence of the reciprocal magnetic susceptibilities for BaLn$_2$FeS$_5$ below 300 K. A "bend" in the linear slope of the χ^{-1}–T curve between 50 and 300 K is observed at 120 K for Ln = Ce, at 150 K for Ln = Pr,

Table 1. The Effective Magnetic Moments μ_{eff} (μ_{B}) of Fe^{2+} Ion in BaLn$_2$FeS$_5$

	μ_{eff} $(\mu_{\mathrm{B}}$/Fe) $50 \leq T/\mathrm{K} \leq 120$	μ_{eff} $(\mu_{\mathrm{B}}$/Fe) $170 \leq T/\mathrm{K} \leq 300$
BaCe$_2$FeS$_5$	4.47	5.31
BaPr$_2$FeS$_5$	4.48	5.07
BaNd$_2$FeS$_5$	4.53	5.11

at 170 K for Ln = Nd, and at 160 K for Sm. The effective magnetic moment and the Weiss constant were obtained by applying the Curie-Weiss law fitting to the χ^{-1}–T curve in the two temperature ranges of 50 K $\leq T \leq$ 120 K and 170 K $\leq T \leq$ 300 K. The total effective magnetic moment for BaLn$_2$FeS$_5$ should be presented by the following equation, except for the Sm compound,

$$\mu_{\mathrm{eff}}(\mathrm{total})^2 = \mu_{\mathrm{eff}}(\mathrm{Fe}^{2+})^2 + 2\mu_{\mathrm{eff}}(\mathrm{Ln}^{3+})^2. \qquad (1)$$

Previously, we have reported that the effective magnetic moment of the Ln ion in the BaLn$_2$ZnS$_5$ (Ln = Ce, Pr, Nd) compounds is in good agreement with that of a free Ln^{3+} ion.[12] Since the paramagnetic behavior of the Sm^{3+} ion does not obey a simple Curie-Weiss law due to the large Van Vleck paramagnetism, we cannot apply Eq. 1 to the χ^{-1}–T curve for BaSm$_2$FeS$_5$. Thus, for the BaLn$_2$FeS$_5$ (Ln = Ce, Pr, Nd) compounds, we have calculated the effective magnetic moment of the Fe^{2+} ion by subtracting the free Ln^{3+} moment from the total moments. Table 1 lists the effective magnetic moments of the Fe ions. The Fe moments (5.1–5.3 μ_{B}) in the higher temperature range (170 K $\leq T \leq$ 300 K) are larger than the value (4.90 μ_{B}) for the high-spin state ($S = 2$) of the 3d^6 electronic configuration and are smaller than the value (6.71 μ_{B}) calculated by taking into account the contribution of the spin-orbit interaction ($S = 2$, $L = 2$).[17] This result indicates that the Fe^{2+} ion has an unquenched orbital moment; such moments agree with the experimental values reported for other compounds.[18] In the lower temperature range (50 K $\leq T \leq$ 120 K), the Fe moments ($\sim$4.5 μ_{B}) are smaller than the 'spin-only' value in the high-spin 3d^6 state. The Fe ion is in a distorted tetrahedral coordination with four sulfur ions.[13] The 3d orbitals of the Fe^{2+} ions would split into a low-lying e state and an excited t_2 state under the crystal field with the ideal tetrahedral symmetry (T_{d}); in such a case, the 'spin-only' moment is calculated to be 2.83 μ_{B} in the low-spin 3d^6 state ($S = 1$). The experimental value ($\sim$4.5 μ_{B}) is, however, significantly larger than the low-spin moments. Therefore, the reduction of the Fe^{2+} moment in the BaLn$_2$FeS$_5$ (Ln = Ce, Pr, Nd) below 120–170 K is not a spin transition from a high-spin state to a low-spin state that is sometimes found for the Fe^{3+} compounds, because when the Fe^{2+} ion is tetrahedrally coordinated by four anions, it is not usually in a low-spin state. This moment-reduction will be discussed later in the section of ^{57}Fe Mössbauer spectra.

Electrical Resistivity. The electrical resistivity of BaLn$_2$FeS$_5$ (Ln = Ce, Pr, Nd, Sm) is plotted in Fig. 3 as a function of the reciprocal temperature. All the compounds indicate an increase in their resistivities with decreasing temperature, and the resistivities show two different Arrhenius temperature-dependencies, one in the at high temperature region
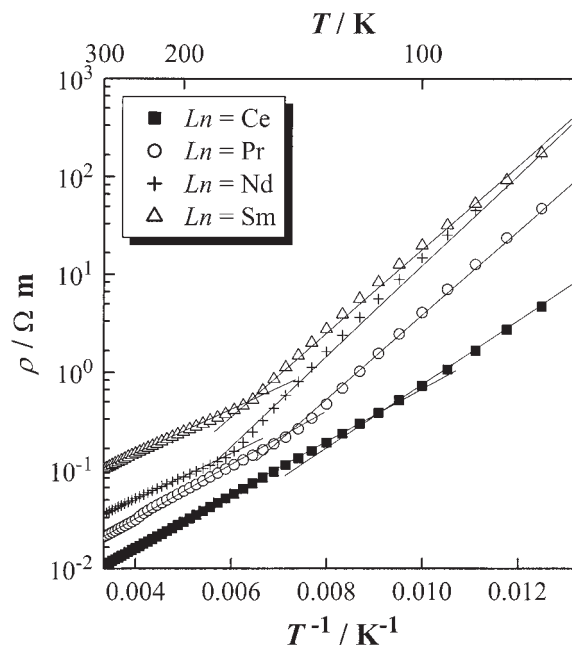

Fig. 3. Plots of electrical resistivity vs reciprocal temperature for BaLn$_2$FeS$_5$ (Ln = Ce, Pr, Nd, Sm). Solid lines represent the Arrhenius fittings (see text).

Table 2. The Activation Energies E_{a} of BaLn$_2$FeS$_5$ (Ln = Ce, Pr, Nd, Sm) in the High and Low Temperature Ranges

	E_{a}(low)/meV	E_{a}(high)/meV	ΔE_{a}/meV
BaCe$_2$FeS$_5$	121	105	16
BaPr$_2$FeS$_5$	167	104	63
BaNd$_2$FeS$_5$	174	89.2	85
BaSm$_2$FeS$_5$	169	88.5	81

and a different one in the low temperature region. The resistivity values show a "bend" at the corresponding temperature (120–170 K) at which an anomaly has been observed in the temperature dependence of their magnetic susceptibilities. Table 2 lists the activation energies obtained for these compounds in both the high (170 K $\leq T \leq$ 300 K) and low temperature (70 K $\leq T \leq$ 120 K) regions. The activation energy at high temperatures (E_{a}(high) = 90–105 meV) is lower than that at low temperatures (E_{a}(low) = 120–175 meV) and the change in the activation energy $\Delta E_{\mathrm{a}} = E_{\mathrm{a}}$(low) $- E_{\mathrm{a}}$(high) increases in the order of Sm $\sim$ Nd $>$ Pr $>$ Ce.

Specific Heats. Figure 4 shows the temperature dependence of the specific heats for BaLn$_2$FeS$_5$ (Ln = Ce, Pr, Nd, Sm). For all the compounds, a specific heat anomaly (arrows in Fig. 4) has been observed at the corresponding temperature at which a "bend" is found both in the χ^{-1}–T curves of Fig. 2(b) and in the log ρ–T^{-1} curves in Fig. 3. This drop of the specific heat with increasing temperature suggests a transformation of the crystal structure at the anomaly temperature.

Another specific heat anomaly has been also found below ca. 40 K. In order to estimate the magnetic contribution to its specific heat anomaly, we have measured the specific heat for a nonmagnetic BaLa$_2$ZnS$_5$. The specific heat data for BaLa$_2$ZnS$_5$, which is isostructural with BaLn$_2$FeS$_5$, are also plotted in the same figure (Fig. 4). If we assume that the elec-

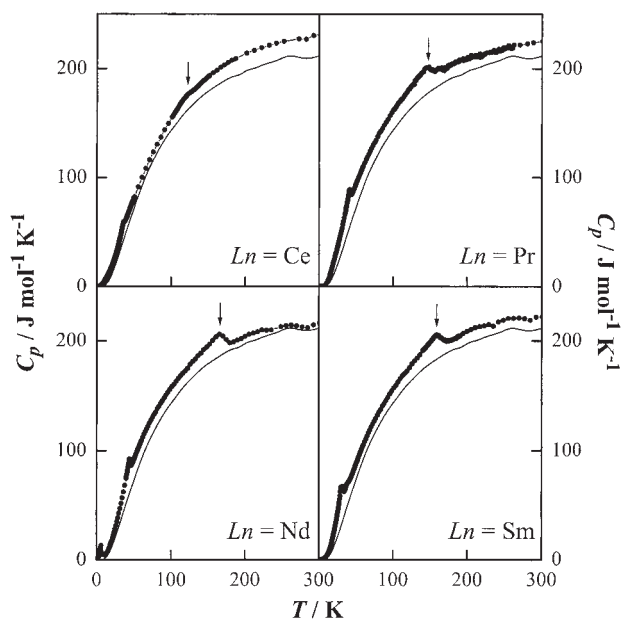Fig. 4. Temperature dependence of specific heats for BaLn$_2$FeS$_5$ (Ln = Ce, Pr, Nd, Sm). The specific heat for diamagnetic BaLa$_2$ZnS$_5$ is shown with a solid line (see text).
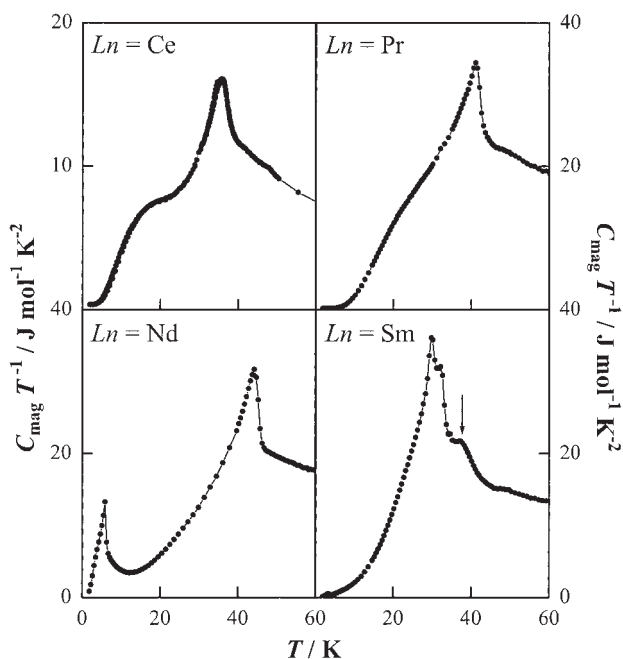
Fig. 5. Magnetic specific heat divided by temperature (C_{mag}/T) for BaLn$_2$FeS$_5$ (Ln = Ce, Pr, Nd, Sm) as a function of temperature at 50, 100, 200, and 300 K.

tronic and lattice contributions to the specific heat for BaLa$_2$ZnS$_5$ and for BaLn$_2$FeS$_5$ are equal, the magnetic specific heat for BaLn$_2$FeS$_5$ is obtained by subtracting the specific heat of BaLa$_2$ZnS$_5$ from that of BaLn$_2$FeS$_5$. The temperature dependence of the magnetic specific heats for BaLn$_2$FeS$_5$ is plotted in Fig. 5. For any of the Ce, Pr, and Nd compounds, a λ-type specific heat anomaly at around 40 K has been observed; it should be due to an antiferromagnetic ordering of

Fe^{2+}.

The ground states of Ce^{3+}, Pr^{3+}, Nd^{3+}, and Sm^{3+} ions are $^2F_{5/2}$, $^3H_4$, $^4I_{9/2}$, and $^6H_{5/2}$, respectively; they are Kramers' ions except for the case of Pr^{3+} ion. Consequently, the ground levels of the Ce, Nd, and Sm ions should be a Kramers' doublet under a tetragonal symmetry, and are expected to show a magnetic ordering of the Ln^{3+} moments or a Schottky-like anomaly due to a Zeeman splitting of the Ln^{3+} ground doublet by the Fe^{2+} molecular field at low temperatures.

Figure 5 shows that the specific heat of the BaCe$_2$FeS$_5$ has a broad shoulder due to a Schottky-like anomaly below 25 K and that another antiferromagnetic ordering has appeared at 5.9 K for of BaNd$_2$FeS$_5$. Considering the results of magnetic susceptibility measurements (Fig. 2), we can attribute the λ-type anomaly at 5.9 K for the Nd compound to an antiferromagnetic transition of Nd^{3+}. In the magnetic specific heat vs temperature curve, the BaSm$_2$FeS$_5$ compound has a broad peak at around 40 K (see the arrow in Fig. 5) and a λ-type peak at about 30 K. On the analogy of the magnetic behavior for the Ce, Pr, and Nd compounds, the two specific heat peaks observed at 30 and 40 K are considered to correspond to the antiferromagnetic orderings of the Sm and Fe ions, respectively.

Crystal Structure at Low Temperatures.   Low-temperature X-ray diffraction measurements for BaPr$_2$FeS$_5$ were carried out below 300 K. All the diffraction patterns in the temperature range from 15 to 300 K were indexed on a tetragonal structure with the space group $I4/mcm$, and no phase transition was observed in the experimental temperature range. Figure 6 shows the variation of the lattice parameters, a and c, as a function of temperature. The variation of the c value with temperature shows an anomaly at around 150 K, while the a value increases monotonously with temperature. For a series of BaLn$_2$TS$_5$ (Ln = La–Nd, T = Mn, Co, Zn, Fe), the increase in the a values is mainly due to the lanthanide size, and that of the c values is due to the transition metal size.[10,12] Thus, the anomaly for the c value is presumably due to the change in the Fe–S bond lengths and/or the S–Fe–S bond angles. This anomaly corresponds to the anomalies observed at 120–170 K from the magnetic susceptibility, specific heat, and electrical
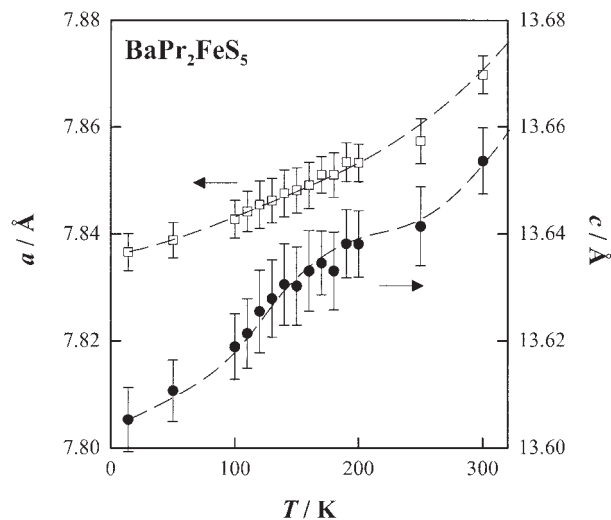

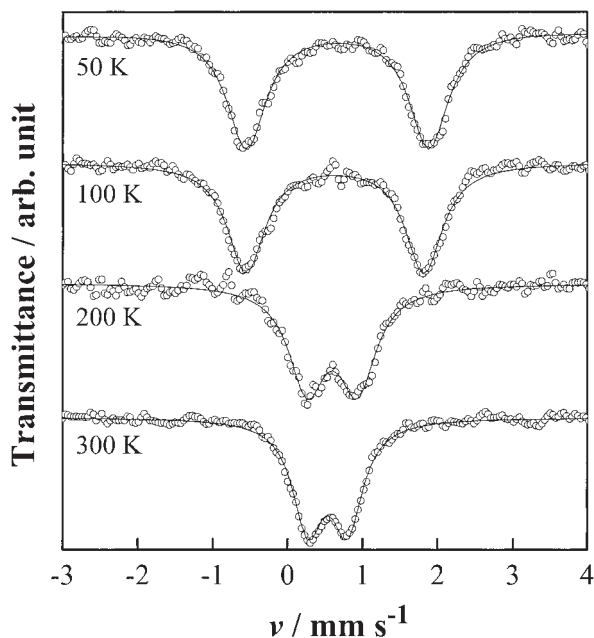Fig. 6. Variation of lattice parameters as a function of temperature for BaPr$_2$FeS$_5$.

Fig. 7. Mössbauer spectra at 50, 100, 200, and 300 K for BaPr$_2$FeS$_5$.

Fig. 8. Temperature dependence of quadruople splittings (Δ) for BaPr$_2$FeS$_5$.

resistivity measurements.

^{57}Fe Mössbauer Spectra.   In order to discuss the anomaly at around 150 K, the Mössbauer spectrum measurements for BaPr$_2$FeS$_5$ were carried out at various temperatures in the temperature range between 50 and 300 K. Figure 7 shows ^{57}Fe Mössbauer spectra at 50, 100, 200, and 300 K. The isomer shift observed at 300 K is ~0.55 mm/s. The Fe^{2+} ions coordinated by four sulfur ions in a high-spin state show the isomer shift in the range of 0.4–0.7 mm/s.[19–21] This result indicates that the Fe ion in the BaPr$_2$FeS$_5$ is divalent in a high-spin state, which is consistent with the results provided by the magnetic susceptibility measurements in the higher temperature range (170 K $\leq T \leq$ 300 K). In this compound, the Fe ions occupy an equivalent lattice site. A doublet due to a quadrupole interaction is observed in all the spectra; the splitting widths between two peaks are found to become wider at lower temperatures. The temperature dependence of the quadrupole splitting (Δ) is plotted in Fig. 8. The quadrupole splittings increase with decreasing temperature and an abrupt drop is observed in the temperature range from 100 to 170 K. Since the quadrupole splittings depend on the distortion of the local coordination environment around the central metal ion, the increase in the quadrupole splitting indicates some distortion of the FeS$_4$ tetrahedron. This FeS$_4$ distortion splits the ground term of the Fe^{2+} ion into non-degenerate states, which should be expected to quench the orbital contributions to the Fe^{2+} magnetic moment.[17]

Magnetic Structure.   To determine the magnetic structure for BaPr$_2$FeS$_5$ at lower temperatures, we have performed powder neutron diffraction measurements. Figure 9 shows the diffraction patterns measured at 10, 100, and 200 K. The patterns at 100 and 200 K were indexed on a tetragonal structure with the space group $I4/mcm$. Their crystallographic parameters were refined by the Rietveld method and the parameters are listed in Table 3.
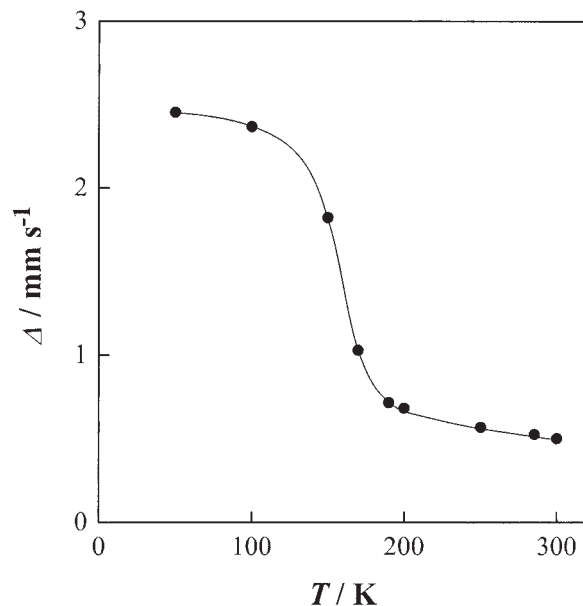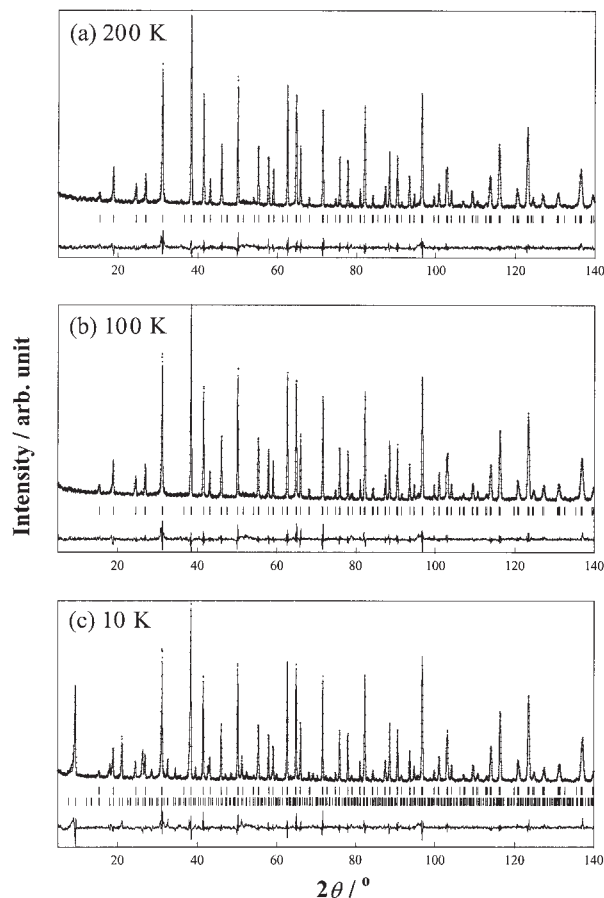

Fig. 9. Neutron diffraction patterns for BaPr$_2$FeS$_5$ at 200 K(a), 100 K(b) and 10 K(c). The calculated and observed diffraction patterns are shown on the top solid line and cross markers, respectively. The vertical marks in the middle show positions calculated for Bragg reflections. The bottom trace is a plot of the difference between calculated and observed intensities.

Table 3. Crystal and Magnetic Data Determined by Neutron Diffraction at 200, 100 and 10 K

	Site	x	y	z	$B/\text{Å}^2$	m/μ_B
200 K	Space group:$I4/mcm$			$a = 7.8357(1)$ Å, $c = 13.6037(3)$ Å		
	$R_{wp} = 11.05\%$, $R_I = 4.46\%$					
Ba	$4a$	0	0	1/4	0.55(5)	
Pr	$8h$	0.1628(2)	0.6628	0	0.63(6)	
Fe	$4b$	0	1/2	1/4	0.70(4)	
S(1)	$4c$	0	0	0	0.70(10)	
S(2)	$16l$	0.1505(3)	0.6505	0.6348(2)	0.93(6)	
100 K	Space group:$I4/mcm$			$a = 7.8298(1)$ Å, $c = 13.5915(3)$ Å		
	$R_{wp} = 11.90\%$, $R_I = 4.92\%$					
Ba	$4a$	0	0	1/4	0.36(5)	
Pr	$8h$	0.1623(2)	0.6623	0	0.58(5)	
Fe	$4b$	0	1/2	1/4	0.49(3)	
S(1)	$4c$	0	0	0	0.52(9)	
S(2)	$16l$	0.1501(3)	0.6501	0.6344(2)	0.63(5)	
10 K	Space group:$I4/mcm$			$a = 7.8217(1)$ Å, $c = 13.5755(3)$ Å		
	$R_{wp} = 11.05\%$, $R_I = 4.46\%$					
Ba	$4a$	0	0	1/4	0.11(5)	
Pr	$8h$	0.1624(3)	0.6624	0	0.43(6)	
Fe	$4b$	0	1/2	1/4	0.42(3)	2.78(2)
S(1)	$4c$	0	0	0	0.35(10)	
S(2)	$16l$	0.1500(3)	0.6500	0.6349(2)	0.59(5)	

$R_{wp} = \left[\sum w(|F(o)| - |F(c)|)^2 / \sum w|F(o)|^2\right]^{1/2}$, $R_I = \sum |I_k(o) - I_k(c)| / \sum I_k(o)$.

For $BaPr_2FeS_5$, the Fe ions have been found to be in an antiferromagnetic state below ca. 40 K through its magnetic susceptibility and specific heat measurements. In the neutron diffraction pattern at 10 K, a number of low-angle peaks for magnetic reflections which were not observed at 100 K and 200 K appear (see Fig. 9(c)), indicating the existence of a long-range antiferromagnetic ordering of the Fe^{2+} moments. Figure 10 shows the detailed diffraction patterns in the angles of $2\theta = 5$–$40°$. These magnetic Bragg reflections {$h/2\ k/2\ l$} are indexed as h, $k =$ odd and $l =$ even, and are consistent with a magnetic configuration with a propagation vector $\boldsymbol{k} = (1/2, 1/2, 0)$. Therefore, considering the magnetic orderings of Fe^{2+}, one can conclude that the magnetic unit cell at 10 K should have dimensions $\sqrt{2}a \times \sqrt{2}a \times c$ in terms of the tetragonal chemical cell. By the Rietveld analysis, the magnetic moment has been refined to be $m = 2.78(2)\ \mu_B$, and has been determined to orient along the c axis. The schematic crystal and magnetic structure of $BaPr_2FeS_5$ at 10 K is illustrated in Fig. 11. The refined magnetic moment of Fe^{2+} in $BaPr_2FeS_5$ is significantly smaller than the moment expected for the high-spin Fe^{2+} moment of $4\ \mu_B$ and is pronouncedly larger than the moment expected for the low-spin moment of $2\ \mu_B$.

Conclusions

Magnetic and electrical properties of quaternary iron sulfides, $BaLn_2FeS_5$ (Ln = Ce, Pr, Nd, Sm), have been investigated. An antiferromagnetic transition due to the Fe^{2+} ions was found to occur at ca. 40 K for each compound. The Nd^{3+} and Sm^{3+} ions also showed an antiferromagnetic ordering at 6.5 K and 28 K, respectively. For all the compounds, another anomaly was observed at 120–170
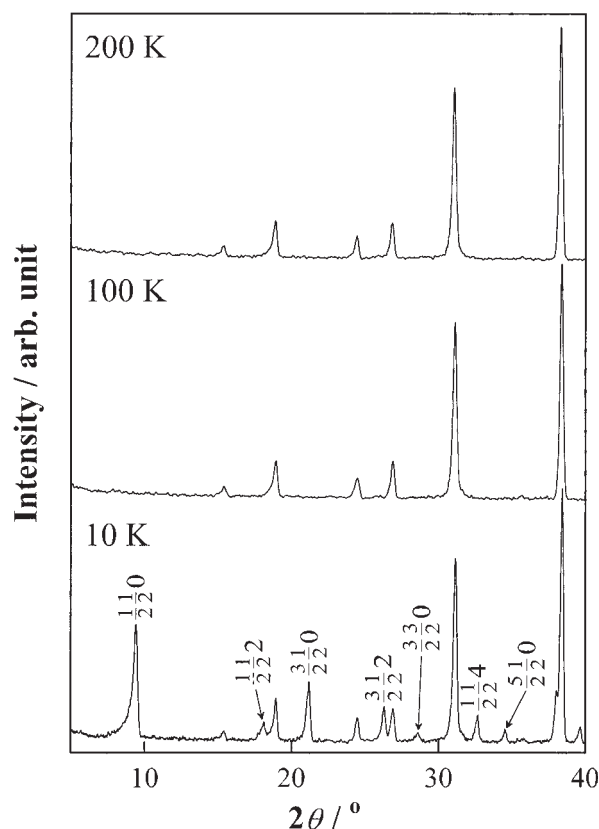

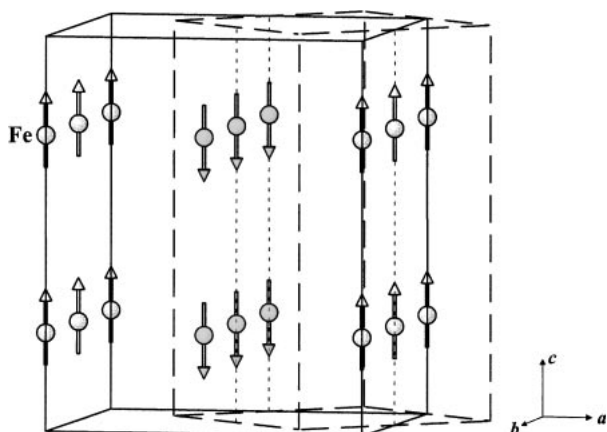Fig. 10. Neutron diffraction patterns for $BaPr_2FeS_5$ at 200 K, 100 K and 10 K in the range of $2\theta = 25$–$40°$.

Fig. 11. Magnetic structure of Fe^{2+} in $BaPr_2FeS_5$ with a $\sqrt{2}a \times \sqrt{2}a \times c$ unit cell at 10 K. Arrows indicate the orientation of the Fe^{2+} moments. Broken lines present the unit cell of the crystal structure.

K in the temperature dependence of the magnetic susceptibilities, electrical resistivities, and specific heat. The low temperature X-ray diffraction and Mössbauer spectrum measurements suggest that this anomaly is associated with the distortion of the FeS_4 tetrahedron.

References

1   J. Flahaut and P. Laruelle, in L. Eyring (ed.), "Progress in the Science and Technology of the Rare Earths," Pergamon Press, Oxford (1968), Vol. 3, pp. 149–283.

2   J. Flahaut, in K. A. Gschneidner Jr. and L. R. Eyring (eds.), "Handbook on the Physics and Chemistry of Rare Earths," North-Holland Publishing Company, Amsterdam, New York, Oxford (1979), Vol. 4, pp. 1–88.

3   P. M. van Calcar and P. K. Dorhout, *Mater. Sci. Forum.*, **315–317**, 322 (1999).

4   W. Ping and J. A. Ibers, *J. Solid State Chem.*, **107**, 347 (1993).

5   W. Ping, A. E. Christuk, and J. A. Ibers, *J. Solid State Chem.*, **110**, 337 (1994).

6   W. Ping and J. A. Ibers, *J. Solid State Chem.*, **110**, 156 (1994).

7   R. L. Gitzendanner, C. M. Spencer, F. J. DiSalvo, M. A. Pell, and J. A. Ibers, *J. Solid State Chem.*, **131**, 399 (1997).

8   P. Stoll, P. Durichen, C. Nather, and W. Bensch, *Z. Anorg. Allg. Chem.*, **624**, 1807 (1998).

9   H. Masuda, T. Fujino, N. Sato, and K. Yamada, *J. Solid State Chem.*, **146**, 336 (1999).

10   M. Wakeshima and Y. Hinatsu, *J. Solid State Chem.*, **153**, 330 (2000).

11   M. Wakeshima, Y. Hinatsu, K. Oikawa, Y. Shimojo, and Y. Morii, *J. Mater. Chem.*, **10**, 2183 (2000).

12   M. Wakeshima and Y. Hinatsu, *J. Solid State Chem.*, **159**, 163 (2001).

13   K. Ino, M. Wakeshima, and Y. Hinatsu, *Mater. Res. Bull.*, **36**, 2207 (2001).

14   M. Wakeshima, K. Ino, and Y. Hinatsu, *Solid State Commum.*, **120**, 145 (2001).

15   Y. Morii, *J. Cryst. Soc. Jpn.*, **34**, 62 (1992).

16   F. Izumi, "The Rietveld Method," ed. by R. A. Young, Oxford University Press, Oxford (1995).

17   A. Weiss and H. Witte, "Magnetochmie," Verlag Chemie GmbH, Weinheim (1973).

18   A. Earnshaw, "Introduction to Magnetochemistry," Academic Press, London (1968).

19   N. N. Greenwood and T. C. Gibb, "Mössbauer Spectroscopy," Chapman and Hall, London (1971).

20   W. M. Reiff, I. E. Grey, A. Fan, Z. Eliezer, and H. Steinfink, *J. Solid State Chem.*, **13**, 32 (1975).

21   J. T. Hoggins and H. Steinfink, *Inorg. Chem.*, **15**, 1682 (1976).